Study of Polyamide 1212/Polyamide 6 Composites with Microfiber Structure via in-Situ Anionic Polymerization

Yulin Li,*,†,‡,§ Vincent Ferreiro,‡ Tingxiu Xie,§ and Guisheng Yang§

Biomaterials Center, National Institute for Materials Science, 1-1 Namiki, Tsukuba, Ibaraki 305-0044, Japan; Laboratoire de Structure et Propriétés de l'Etat Solide (L.S.P.E.S.), Université des Sciences et Technologies de Lille (USTL) Bât. C6, Rue Paul Langevin 59655 Villeneuve d'Ascq, France; and Joint Laboratory of Polymer Science and Materials, Institute of Chemistry, Chinese Academy of Sciences, Beijing 100080, P. R. China

Received June 4, 2007; Revised Manuscript Received July 14, 2007

ABSTRACT: A series of novel PA 1212/PA 6 composites were synthesized via in-situ polymerization. Incorporating minor PA 1212 (2−12 wt %) into PA 6 matrix led to about 5 times increase of impact resistance of PA6 with its tensile strength maintenance. Inserting PA 1212 macromolecules into PA 6 matrix by this method may interfere with the arranging order of hydrogen bonding of PA 6 by changing its crystalline structure and impeding its crystallization. Different from the homogeneous molecular PA 66/PA 6 composites, PA 1212/PA 6 composites had a microfiber structure with width 100−300 nm and length several micrometers. PA 1212/PA 6 composites had better crystalline thermal stability and comprehensive mechanical properties than the corresponding molecular PA 66/PA 6. After tensile deformation, the lamellar bundles in PA 1212/PA 6 had a prior orientation along the tensile direction, while the orientation direction in pure PA 6 had an angle about 45° with the tensile direction. The crystalline microstructure and morphology of PA 1212/PA 6, especially the microfibers, might play an important role in the toughening of PA 6 with maintenance of strength.

Introduction

As a high-performance engineering plastic, polyamide 6 (PA 6) has high strength, good fatigue resistance, and wearing durability due to the existence of strong intermolecular hydrogen-bonding interaction. Nevertheless, PA 6 has relatively poor notched Izod impact toughness and tensile properties at room temperature, which greatly restricted the applications in aerospace, auto industries, drawn fibers, and films.[1−3] In contrast, polyethylene has high drawability because the absence of specific intermolecular interactions leads to the crystal deformation through slippage along the crystallographic planes. These results suggest that the transfer of stress within PA 6 can be improved by adjustment of the intensity of its interchain interactions, which might lead to effective energy dissipation and result in the efficient improvement of its tensile deformation and impact resistance.

In spite of their similar structure, polyamide 66 and polyamide 6 tend to crystallize separately in their blends prepared by a simple blending method.[4] We hypothesized that the strong hydrogen bonding between polyamide and ϵ-caprolactam monomer and between the polyamides might overcome the phase separation problem caused by the reduction of ΔS_{mix} after polymerization. In our previous studies,[5] a series of PA 6 molecular composites with polyamide 66 (PA 66) were synthesized via in-situ anionic polymerization of ϵ-caprolactam with PA 66 soluble in it. It was found that the strong hydrogen-bonding interactions during in-situ polymerization process led to the molecular dispersion of PA 66 into PA 6.

In this study, a polyamide with long alkane segments, polyamide 1212 (PA 1212) with lower hydrogen-bonding strength compared with that of PA 66, was introduced into PA 6 to form PA 1212/PA 6 composites with microfiber structure different from molecular PA 66/PA 6 composites[5] via a similar approach. The mechanical and impact properties were studied. The morphologies, crystallization properties and crystalline structure, and hydrogen-bonding interaction were investigated with scanning electron microscope (SEM), polarized microscope, atomic force microscope (AFM), differential scanning calorimeter (DSC), X-ray diffraction analyzer (WAXD), and FTIR spectrometer, respectively.

Experimental Section

Materials. PA 1212 was supplied by Shangdong Dongchen Chemical Co., China. ϵ-Caprolactam was provided by Nanjing Oriental Chemical Co., China. Sodium hydrate (NaOH) and toluene diisocyanate (TDI) were obtained from Shanghai Chemical Reagents Co. China National Medicines, China.

Synthesis of PA 1212/PA 6 Composites. PA 1212 was dissolved in melted ϵ-caprolactam monomer at 180 °C under nitrogen to form a homogeneous transparent polymer−monomer solution. The solution was vacuumed at 170 °C for about 20 min to remove water. Then 0.17 wt % NaOH was added under stirring and continuously vacuumed for another 10 min. After this 0.4 wt % TDI was added with stirring; the mixture was then immediately poured into a mold preheated to 180 °C and polymerized in oven at 180 °C for 20 min. After polymerization, the products were cooled to room temperature, extracted with boiling water to eliminate the residual monomer, and then vacuum-dried at 80 °C for 10 h. At last, the PA 1212/PA 6 composites with different PA 1212 content were obtained, which will be denoted as "PA 1212/PA 6" below for short.

Preparation of PA 1212/PA 6 Blend Sample and Pure PA 1212 Sample. As control samples, coextruded PA 1212/PA 6 and pure PA 1212 samples were prepared by a 35 twin-screw extruder (SHJ-30) at a screw speed of 240 rpm and barrel temperatures 220−225−230−230−230 °C. The pelletized materials will be denoted as "Blend PA 1212/PA 6" and "PA 1212" later.

Characterization. The molecular weight of PA 6 of pure PA 6, PA 1212/PA 6, PA 66/PA6 (synthesized in our previous study[5])

* Corresponding author: Fax +81 (0) 29-860-4714; e-mail yulin@iccas.ac.cn.
† National Institute for Materials Science.
‡ Université des Sciences et Technologies de Lille.
§ Chinese Academy of Sciences.

10.1021/ma071237j CCC: $37.00
Published on Web 10/09/2007

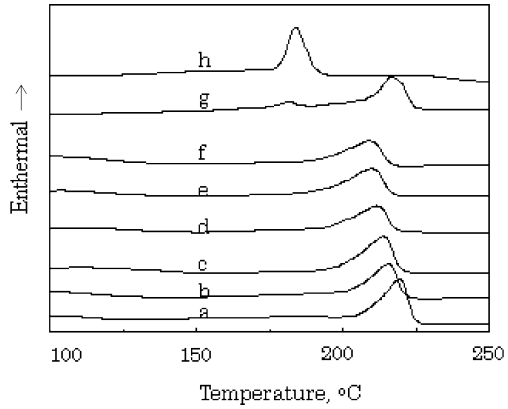

Figure 1. (A) DSC curves of PA 1212/PA 6 composites containing (a) 0 wt % PA 1212, (b) 2 wt % PA 1212, (c) 4 wt % PA 1212, (d) 6 wt % PA 1212, (e) 8 wt % PA 1212, (f) 10 wt % PA 1212, (g) blend sample with 10 wt % PA 1212, and (h) pure PA 1212.

was analyzed by gel permeation chromatography (GPC, HLC-8120, TOSOH Co., Japan) using 3-methylphenol as solvent and standard polyamide 6 for calibration. In order to eliminate process history effect, PA 1212/PA 6, Blend PA 1212/PA 6, PA 1212, and PA 66/PA 6 were hot pressed into sheets with $50 \times 50 \times 3$ mm^3 at 30 MPa and 250 °C (preheating the samples at 250 °C for 10 min before press) and cooled to room temperature for further characterization. The sheets were cut into standard specimens for tensile and impact testing. The tensile testing (five samples for each point) was performed on a Shimadzu AGH-1kN universal testing machine according to ASTM D638 with strain rate of 60 mm/min at room temperature. The Izod notched impact strength (10 samples for each point) was measured with an XJU-22 impact testing machine according to ASTM D256 at room temperature. The surfaces of freeze-fractured samples in liquid nitrogen and those of impact-fractured specimens at room temperature were observed on a JSM-5600LV scanning electron microscope after they were gold-coated in a vacuum chamber. The orientation of tensile samples was observed on an Olympus BX51-33P-OC-SP polarized microscope. The surfaces of undeformed and deformed samples were observed on an AFM (Nanoscope III-a, Digital Instruments Ltd.) using a tapping mode. DSC measurements were performed on a Perkin-Elmer Pyris-1 differential scanning calorimeter (DSC) from room temperature to 250 °C at a heating rate of 10 °C /min under a nitrogen atmosphere. X-ray diffraction spectra were collected on a Rigaku D/Max-III X-ray diffraction (XRD) analyzer equipped with a rotating-anode generator system using Cu Kα (λ = 1.54 Å) radiation at an operating current of 25 mA and a voltage of 35 kV. The scanning rate was 1°/min. The films for FTIR analysis were prepared and examined on a Perkin-Elmer Spectrum 2000 spectrometer according to ref 5. The thickness of the films ensured the intensity of bands in the range of Beer−Lambert law. The temperature was increased at a speed of 2 °C/min, and the data were collected at an interval of 20 °C.

Table 1. Molecular Weight of PA 6 in PA1212/PA 6 and PA 66/PA 6 Composites

PA 1212 content (wt %)	M_n ($\times 10^4$)	M_w ($\times 10^4$)	M_w/M_n
0	4.52 ± 0.01	9.98 ± 0.01	2.21
6	4.47 ± 0.01	9.87 ± 0.01	2.20
10	4.22 ± 0.01	9.14 ± 0.01	2.17
10[a]	4.33 ± 0.01	9.24 ± 0.01	2.13

[a] PA 66/PA 6 containing 10 wt % PA 66.

Results and Discussion

The molecular weight of PA 6 in PA 1212/PA 6 and PA 66/PA 6 is shown in Table 1.

Figure 1 shows the DSC curves of PA 1212/PA 6 composites with different PA 1212 content and the corresponding Blend PA 1212/PA 6. Single melting peak was observed for all PA 1212/PA 6 with different PA 1212 content, while two melting peaks in Blend PA 1212/PA 6 were detected. Up to now, we can get a temporary conclusion that the added PA 1212 is not crystallized but dispersed in PA 6 matrix in an amorphous state.

After incorporating PA 1212 into PA 6, the glass transition temperature T_g, the melt enthalpy ΔH_f, the melting temperature T_m, and the crystallization temperature T_c of PA6 in PA 1212/

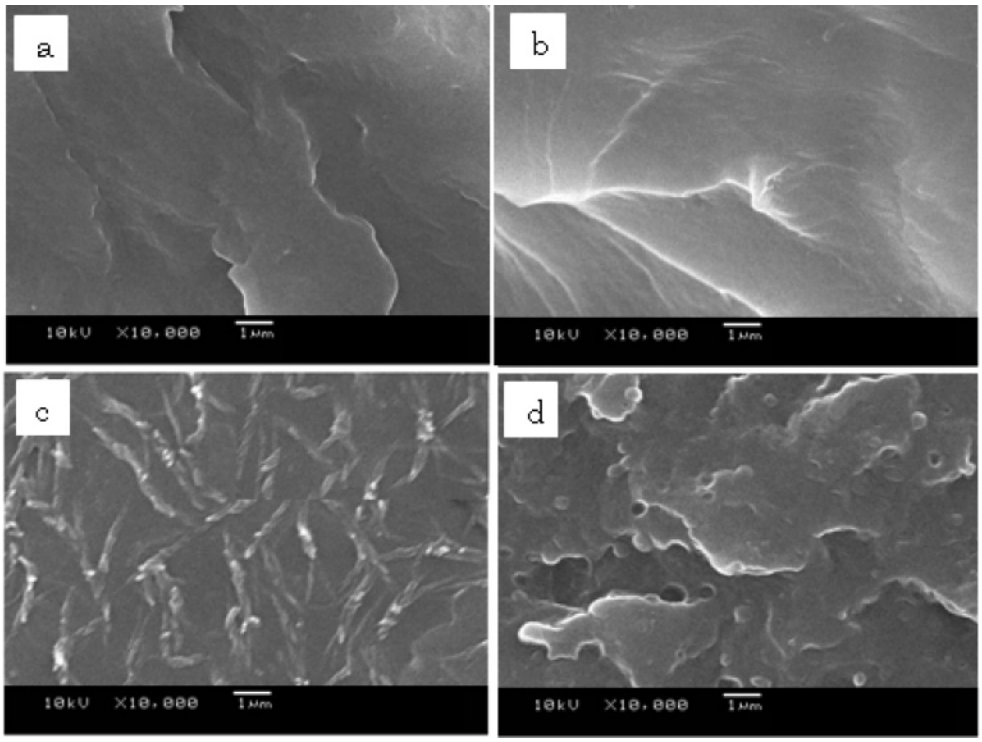

Figure 2. SEM photographs of freeze-fractured surfaces of (a) pure PA 6, (b) PA 66/PA 6 with 10 wt % PA 66, (c) PA 1212/PA 6 with 10 wt % PA 1212, and (d) blend PA 1212/PA 6 with 10 wt % PA 1212.

Table 2. Melting and Crystallization Behavior of PA1212/PA 6 and Comparison Materials

PA 1212 cont (%)	T_g (°C)	T_m (°C)	ΔH_f (J/g)	T_c (°C)
0	61.2 ± 0.1	220.0 ± 0.1	65.1 ± 0.05	173.2 ± 0.1
2	55.3 ± 0.1	217.3 ± 0.1	63.6 ± 0.05	169.7 ± 0.1
4	56.7 ± 0.1	217.1 ± 0.1	60.3 ± 0.05	167.7 ± 0.1
6	55.4 ± 0.1	213.1 ± 0.1	59.1 ± 0.05	165.1 ± 0.1
8	53.1 ± 0.1	209.8 ± 0.1	61.0 ± 0.05	161.1 ± 0.1
10	53.2 ± 0.1	206.8 ± 0.1	60.5 ± 0.05	157.4 ± 0.1
12	51.2 ± 0.1	208.2 ± 0.1	61.2 ± 0.05	156.6 ± 0.1
10[a]	55.2 ± 0.1	219.8 ± 0.1	64.9 ± 0.05	172.1 ± 0.1
		183.1 ± 0.1[c]	30.1 ± 0.05[c]	
10[b]	48.5 ± 0.1	197.1 ± 0.1	42.7 ± 0.05	153.1 ± 0.1
pure 1212	53.1 ± 0.1[d]	188.6 ± 0.1[d]	62.61 ± 0.05[d]	161.9 ± 0.1[d]

[a] Blend PA 1212/PA 6 containing 10 wt % PA 1212. [b] PA 66/PA 6 containing 10 wt % PA 66. [c] T_m and ΔH_f of PA 1212 in Blend PA 1212/PA 6 containing 10 wt % PA 1212. [d] T_g, T_m, ΔH_f, and T_c of pure PA 1212.

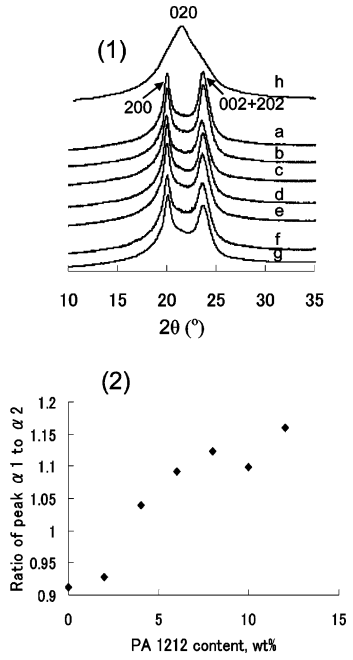

Figure 3. (1) XRD intensity profile of PA 1212 /PA 6 as a function of PA 1212 content: (a) 0, (b) 2, (c) 4, (d) 6, (e) 8, (f) 10, (g) 12 wt %, (h) pure PA 1212. (2) Ratio of the intensity of peak α_1 to peak α_2 with increasing PA 1212.

PA 6 decreased, and the width of T_m became broader, indicating that the crystallinity of PA 6 in PA 1212/PA 6 decreased and its crystallization was more incomplete. In other words, PA 1212 molecules impeded the crystallization behavior of PA 6 (Table 2).

The SEM image of PA 1212/PA 6 composite showed some interentangled fiberlike structure in the matrix compared to the homogeneous morphologies of pure PA 6 and PA 66/PA 6 composites and the particle-dispersed morphologies of Blend PA 1212/PA 6 (Figure 2). The fibers had an aspect ratio of 20−30, with width about 100−300 nm and length several micrometers.

Diffraction spectra of pure PA 6 and PA 1212, and PA1212/PA 6 with different PA 1212 content are shown in Figure 3 (1). The peak (020) gave a clear indication of γ crystalline form in pure PA 1212.[6,7] For pure PA 6 and PA1212/PA 6, the α-form was the main crystalline form, showing two main reflections α_1 and α_2, corresponding to the crystallographic planes (200) and (002 + 202).[8] We assume that, similar to the effect of PA 66 on PA 6,[5] the strong interaction between PA 1212 macromolecule and PA 6 macromolecule can result in the conformational changes in chains, limiting the formation of hydrogen-bonded sheets of α phase, which can be verified by the increase of ratio of α_1 diffraction peaks relative to the α_2 diffraction peaks with the addition of PA 1212 (Figure 3(2)).

Table 3. Mechanical Properties of PA 1212/PA 6 with Different PA 1212 Content

PA 1212 cont (wt %)	elongation at break mean ± SD (MPa) (%)	tensile strength mean ± SD (MPa)	notched impact strength mean ± SD (J/m)
0	108.1 ± 3.13	50.8 ± 1.22	102.1 ± 0.54
2	221.2 ± 4.23	61.7 ± 3.12	151.2 ± 1.01
4	324.3 ± 5.21	69.2 ± 2.11	354.2 ± 0.96
6	357.6 ± 2.12	81.2 ± 2.44	370.3 ± 2.12
8	450.2 ± 3.42	88.8 ± 1.01	530.6 ± 1.09
10	441.7 ± 4.32	88.7 ± 2.77	542.1 ± 1.55
12	432.1 ± 2.15	85.6 ± 3.83	556.4 ± 2.24
10[a]	133.1 ± 2.34	48.2 ± 0.55	87.1 ± 0.98
10[b]	443.5 ± 3.45	65.3 ± 2.12	330.2 ± 2.15

[a] Blend PA 1212/PA 6 containing 10 wt % PA 1212. [b] PA 66/PA 6 containing 10 wt % PA 66.

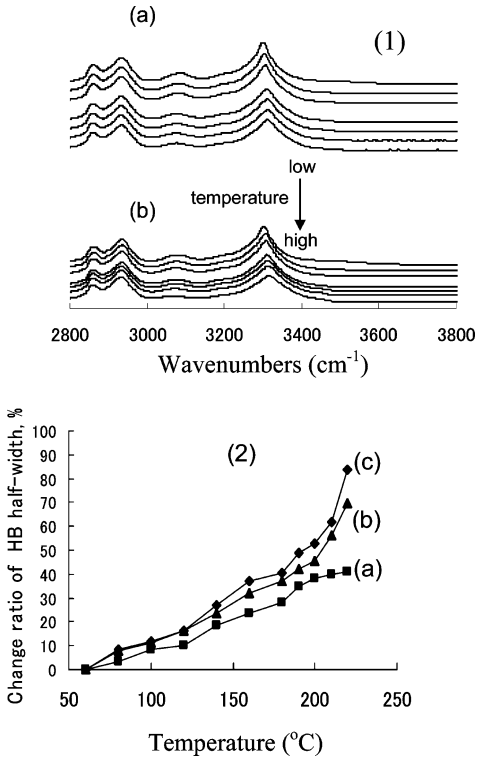

Figure 4. (1) FTIR spectra of N−H stretching region of (a) pure PA 6 and (b) PA 1212/PA 6 containing 10 wt % PA 1212 recorded from 60 to 220 °C in the range of 2800−3800 cm^{-1}. (2) Comparison of the temperature dependence of the half-height width at the hydrogen-bonded N−H stretching based on the corresponding half-height width at room temperature in the range 3100−3500 cm^{-1} (a) pure PA 6, (b) PA 1212/PA 6 containing 10 wt % PA 1212, and (c) PA 6/PA66 containing 10 wt % PA 66.

Figure 4(1) illustrates the FTIR spectra of N−H stretching of PA 6 and PA 1212/PA 6 in the range 3100−3500 cm^{-1}, which were recorded as a function of increasing temperature. It can be seen that the N−H stretching peaks shifted toward high frequency, and the intensity attenuated, the bandwidth became broader with increasing temperature. However, the increase rate of the bandwidth with temperature in pure PA 6 was less than that in PA 1212/PA 6, and the change rate of the bandwidth in PA 1212/PA 6 was less than that in PA 66/PA 6 (Figure 4(2)). This difference reflected that attenuation and

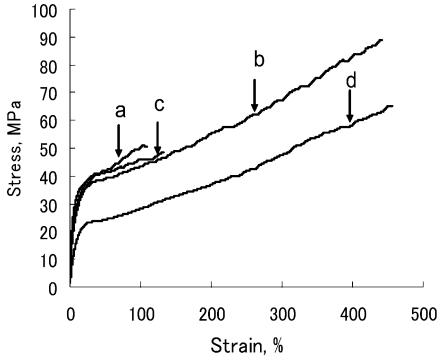

Figure 5. Stress−strain curves for (a) pure PA 6, (b) PA1212/PA 6 containing 10 wt % PA 1212, (c) blend PA1212/PA 6 containing 10 wt % PA 1212, and (d) PA 66/PA 6 containing 10 wt % PA 66.

dissociation of hydrogen bonding with increasing temperature were easiest for PA 66/PA 6, easier for PA 1212/PA 6 compared to pure PA 6. It is assumed that, due to the presence of another polyamide macromolecules in PA 6 matrix, the arranging order of hydrogen bonding of PA 6 was interfered in and became more disordered.[9−11] Because of the more similar structure of PA 66 and PA 6 than that of PA 1212 and PA 6, incorporating PA 66 than PA 1212 into PA 6 would interfere in the arranging order of hydrogen bonding of PA 6 in larger degree and lead to more disordered state in PA 66/PA 6 than that in PA 1212/PA 6, which is in agreement with the lower T_g, ΔH_f, T_m, and T_c of PA6 in PA 66/PA 6 than those of the corresponding PA 1212/PA 6 (Table 2).

The elongation at break of PA 1212/PA 6 increased about 4 times, giving the composites impact strength about 5 times increase (from 102.1 ± 0.54 to 556.4 ± 2.24 J/m) compared with that of the net PA 6, while the tensile strength can keep a good level (Table 3). As contrast, PA 1212 had not obvious effect on the related properties of PA 6 by the blend method. The properties of PA 1212/PA 6 are, to our knowledge, unique, as these materials showed great improvement in toughness with maintenance of strength compared to the large decrease in strength in the corresponding PA 66/PA 6 (Figure 5).

Semicrystalline polyamide 6 does not exhibit individual lamellar structure as in the case of polyethylene, and only lamellar bundles with width about 200 nm were observed.[12] Here, although lamellar bundles with width about 100−200 nm were observed in both pure PA 6 and PA 1212/PA 6, the latter had the lamellar bundles with smaller width and more homogeneous structure compared to pure PA 6 (Figure 6a,c). For tensile sample, the lamellar bundles in PA 1212/PA 6 had a prior orientation along tensile direction, which indicated that slippage of lamellar bundles might occur in PA 1212/PA 6 under tensile deformation (Figure 6d). For deformed PA 6 sample, no orientation of the bundles of lamellae was observed, and the angle about 45° existed between the orientation direction and the tensile direction (Figure 6b). More microfibers were found in PA 1212/PA 6 in contrast with the smooth fractured surface of net PA 6 (Figure 7), which further suggests that quite large deformation happened in the PA 1212/PA 6 composites.

In the case of the PA 1212/PA 6 composites, we postulate that, in contrast to the neat PA 6, the PA 1212 dispersed in PA

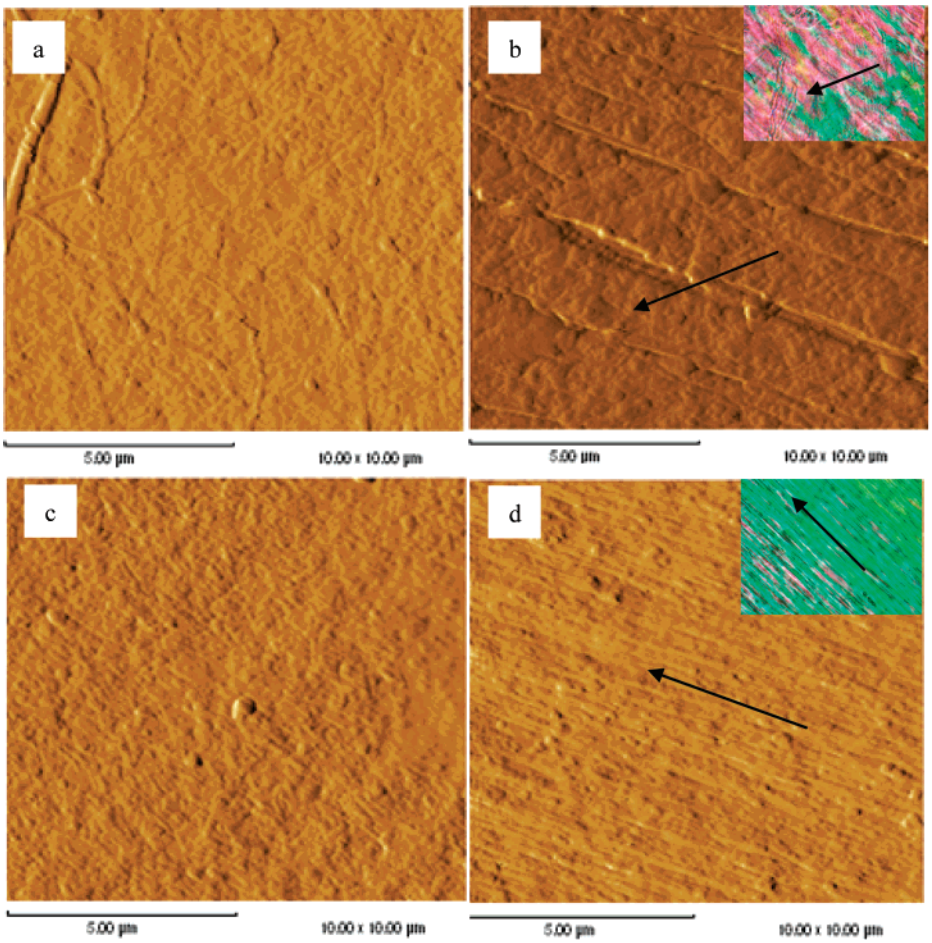

Figure 6. AFM images of surfaces of (a) undeformed and (b) deformed PA 6 and (c) undeformed and (d) deformed PA 1212/PA 6 containing 10 wt % PA 1212; inlet color images are photos obtained from polarized microscope, ×100; black arrows indicate the tensile direction.

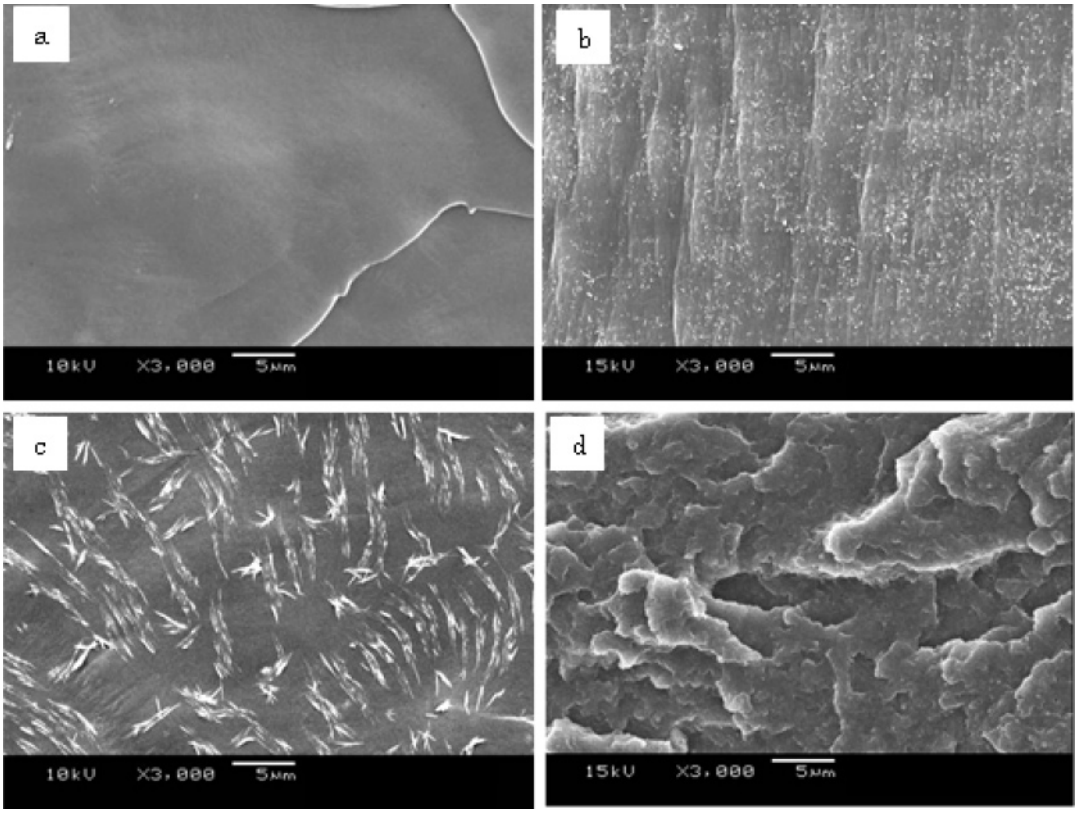

Figure 7. SEM photographs of impact fractured surfaces of (a) pure PA 6, (b) PA 66/PA 6 with 10 wt % PA 66, (c) PA 1212/PA 6 with 10 wt % PA 1212, and (d) blend PA 1212/PA 6 with 10 wt % PA 1212.

6 matrix in a fiberlike amorphous state may lead to a structure much more conducive to plastic flow under applied stress. This might give rise to a more efficient energy-dissipation mechanism in the composites, thereby delaying crack formation caused by the effective stress transfer due to the good interfacial adhesion of the microfibers and the matrix. Because of their large ratio aspect and interentanglement, the microfibers can act as temporary cross-links among the matrix, providing localized regions of enhanced strength, which in turn can retard the growth of cracks.

Conclusion

A series of PA 1212/PA 6 composites with microfiber structure were synthesized via in-situ polymerization. The impact resistance of PA 6 was dramatically improved without sacrificing tensile strength when a small content of PA 1212 (2−12 wt %) was incorporated. Inserting PA 1212 macromolecules into PA 6 matrix by this method may interfere with the arranging order of hydrogen bonding of PA 6, in turn changing its crystalline structure and impeding its crystallization. Compared with molecular PA 66/PA 6 composites, PA 1212/PA 6 had better crystalline thermal stability and comprehensive mechanical properties. Under tensile deformation, the lamellar bundles in PA 1212/PA 6 had a prior orientation along tensile direction, while the orientation direction in pure PA 6 had an angle about 45° with the tensile direction. The crystalline microstructure and morphology of PA 1212/PA 6, especially the microfibers, might play an important role in the toughening of PA 6 with maintenance of its strength.

References and Notes

(1) Boscoletto, A. B.; Trezza, G.; Andreis, B.; Milan, L.; Tavan, M.; Furlan, P. *Macromolecules* **1992**, *25*, 5752.
(2) Ito, M.; Takahashi, A.; Araki, N.; Kanamoto, T. *Polymer* **2001**, *42*, 241.
(3) Galeski, A. *Prog. Polym. Sci.* **2003**, *28*, 1643.
(4) Rybnikář F.; Geil, P. H. *J. Appl. Polym. Sci.* **1993**, *49*, 1175.
(5) Yu, L. L.; Yang, G. S. *Macromol. Rapid Commun.* **2004**, *25*, 1714.
(6) Sikorski, P.; Atkins, E. D. T. *Macromolecules* **2001**, *34*, 4788.
(7) Li, L. B.; Koch, M. H. J.; de Jeu, W. H. *Macromolecules* **2003**, *36*, 1626.
(8) Li, Y.; Yan, D.; Zhu, X. *Macromol. Rapid Commun.* **2000**, *21*, 1282.
(9) Lu, Y. L.; Zhang, G. B.; Feng, M.; Zhang, Y.; Yang, M. S.; Shen, D. Y. *J. Polym. Sci., Part B: Polym. Phys.* **2003**, *41*, 2313.
(10) Skrovanek, D. J.; Howe, S. E.; Painter, P. C.; Colemman, M. M. *Macromolecules* **1985**, *18*, 1676.
(11) Skrovanek, D. J.; Painter, P. C.; Colemman, M. M. *Macromolecules* **1986**, *19*, 699.
(12) Ferreiro, V.; Pennec, Y.; Séguéla, R.; Coulon, G. *Polymer* **2000**, *41*, 1561.

MA071237J